Journal of Sound and Vibration (1997) **202**(2), 235–247

A DUAL BOUNDARY ELEMENT FORMULATION FOR SOUND PROPAGATION AROUND BARRIERS OVER AN IMPEDANCE PLANE

L. A. DE LACERDA

Wessex Institute of Technology, Ashurst Lodge, Ashurst, Southampton SO40 7AA, England and COPPE/UFRJ, Programa de Engenharia Civil, Cx. P. 68506, 21945 *Rio de Janeiro, Brazil*

L. C. WROBEL

Department of Mechanical Engineering, Brunel University, Uxbridge, Middlesex UB8 3PH, England

AND

W. J. MANSUR

COPPE/UFRJ, Programa de Engenharia Civil, Cx. P. 68506, 21945 *Rio de Janeiro, Brazil*

(*Received* 19 *June* 1996, *and in final form* 25 *November* 1996)

In this paper, the Dual Boundary Element Method is formulated and applied to study outdoor sound propagation where acoustic barriers are modelled as non-thickness bodies that may have different impedance conditions at each side. Standard and hypersingular integral equations are applied on each side of the barrier. The infinite impedance plane is incorporated into the Green function in both equations, avoiding the discretization of the ground. Numerical results are presented validating the formulation and the use of non-thickness barriers.

1. INTRODUCTION

The boundary element method has been used to study outdoor sound propagation in a neutral quiescent atmosphere and its abatement by using acoustic barriers for more than 20 years. Seznec [1] used this formulation to study acoustic barriers on a plane rigid ground. Discretization of the ground was avoided by employing the method of images. For the analysis of thin barriers his results were compared with those from geometrical acoustic approaches; good agreement was achieved, and it was concluded that the thickness of the barrier has no effect at all on the excess attenuation, provided that it stays below one wavelength.

If the plane ground is not rigid, the method of images alone is no longer sufficient to generate a Green function that incorporates the absorbing ground. This function was shown to be the solution for a rigid ground with a correction term which is basically an infinite integral with an oscillatory integrand. Many different authors studied the evaluation of this integral for the problem of a point source over a plane impedance boundary and suggested similar asymptotic solutions for the far field [2–5]. Chandler-Wilde and Hothersall [6] developed a similar asymptotic expression for the

0022–460X/97/170235 + 13 $25.00/0/sv960860

two-dimensional case using a modified steepest descent method [7], based in the work of Kawai *et al*. [5] and Brekhovskikh [8], and proposed the use of Gaussian quadrature for the evaluation of the correction term at the near field. Later on, using the boundary element method, they studied the performance of difference barrier profiles over a homogeneous impedance ground [9].

Recently, Park and Eversman [10] studied the same two-dimensional problem for very high frequencies and Chandler-Wilde and Hothersall [11] presented efficient and accurate expressions (except in the very near field) to evaluate the Green function's correction term.

The standard boundary integral equation generally used to study sound attenuation by acoustic barriers [1, 6, 10] cannot be applied alone when the barrier or their attachments are very thin because it produces a degenerate system of equations [12–14]. An alternative for rigid barriers is to use a hypersingular boundary integral equation derived from slender-body theory [15], but this equation also degenerates for very thin, absorbing bodies.

A boundary integral formulation which produces a well-conditioned system of equations when thickness is neglected can be derived by applying a standard boundary integral equation on one side of the thin barrier and a hypersingular boundary integral equation on the other side. This formulation is the basis of the dual boundary element method [16] currently used in fracture mechanics, and which has been applied to acoustic scattering in unbounded regions by Krishnasamy *et al*. [14]. In the present paper, the dual BEM is formulated and applied to the case of sound attenuation by thin absorbing barriers over an impedance plane, with a Green function which incorporates the absorbing ground. It is shown in the applications that this formulation makes discretization easier, reduces computing time and memory requirements and avoids near-singular integrations.

2. MATHEMATICAL FORMULATION AND GREEN FUNCTION

A sketch of the problem of outdoor sound propagation in a homogenous quiescent atmosphere and its attenuation by using thin barriers is shown in Figure 1.

The plane ground is locally reacting and has a homogeneous normalized surface admittance β. The admittance of the barrier surfaces is also locally reacting and may be different on each side depending on the treatment applied.

Linear sound propagation in this medium is described by the Helmholtz equation ($e^{-i\omega t}$ time-dependence)

$$\nabla^2\phi(\mathbf{x}) + k^2\phi(\mathbf{x}) = h(\mathbf{x}), \tag{1}$$

where ϕ is the velocity potential, k is the wavenumber, $h(\mathbf{x})$ is the known source in the domain Ω and ∇^2 is the Laplacian operator. The boundary conditions are represented by

$$q(\mathbf{x}) = \partial\phi(\mathbf{x})/\partial\mathbf{n}(\mathbf{x}) = ik\beta(\mathbf{x})\phi(\mathbf{x}) \tag{2}$$

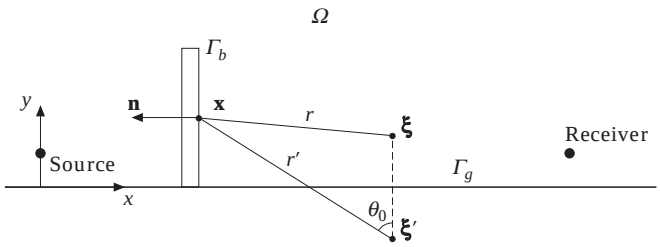

Figure 1. A two-dimensional model of outdoor sound propagation.

for $\mathbf{x}$ on the ground Γ_g or in the barrier Γ_b. $\mathbf{n}$ is the unit outward normal vector at $\mathbf{x}$ and β is the admittance (inverse of the specific acoustic impedance), which may be $\beta = 0$ for a rigid surface or $\mathrm{Re}\,(\beta) \geqslant 0$ for an absorbing one. The velocity potential must also satisfy the Sommerfeld radiation condition at infinity,

$$\lim_{r\to\infty} r^{1/2}(\partial\phi/\partial r - \mathrm{i}k\phi) = 0. \tag{3}$$

In order to avoid discretization of the flat ground a Green function G must be sought which satisfies equations (1)–(3) apart from the boundary condition on the barrier, and where $h(\mathbf{x}) = \delta(\boldsymbol{\xi}, \mathbf{x})$ is the Dirac delta function. If the ground is rigid ($\beta = 0$) it is easy to obtain by using the method of images that

$$G_o(\boldsymbol{\xi}, \mathbf{x}) = -(\mathrm{i}/4)\mathrm{H}_0^{(1)}(kr) - (\mathrm{i}/4)\mathrm{H}_0^{(1)}(kr'), \tag{4}$$

where $\mathrm{H}_\alpha^{(1)}$ is the α order Hankel function of the first kind, r is the distance from the source to the field point and r' is the distance from the image of the source to the field point. Generally, $\beta \neq 0$ and the Green function of interest is the sum of $G_o(\boldsymbol{\xi}, \mathbf{x})$ and a correction term $G_\beta(\boldsymbol{\xi}, \mathbf{x})$:

$$G(\boldsymbol{\xi}, \mathbf{x}) = G_o(\boldsymbol{\xi}, \mathbf{x}) + G_\beta(\boldsymbol{\xi}, \mathbf{x}). \tag{5}$$

The development of an expression for $G_\beta(\boldsymbol{\xi}, \mathbf{x})$ suitable for numerical evaluation has been an object of study by many authors [3–6] and the one used here is that given by Chandler-Wilde and Hothersall [6] which is a two-dimensional version of what has been proposed by Kawai *et al*. [5] in a three-dimensional field. By substituting equation (5) into equation (2) for $\mathbf{x}$ on the ground one finds

$$\partial G_\beta(\boldsymbol{\xi}, \mathbf{x})/\partial y(\mathbf{x}) + \mathrm{i}k\beta G_\beta(\boldsymbol{\xi}, \mathbf{x}) = -(k\beta/2)\mathrm{H}_0^{(1)}(kr'), \tag{6}$$

and by applying direct and inverse Fourier transformation as well as changing the variable of integration the following integral representation is obtained [11]:

$$G_\beta(\boldsymbol{\xi}, \mathbf{x}) = \frac{\mathrm{i}\beta}{2\pi}\int_{-\infty}^{+\infty} \frac{\mathrm{e}^{\mathrm{i}k(\sqrt{1-s^2}(y(\mathbf{x})+y(\boldsymbol{\xi})) - (x(\mathbf{x})-x(\boldsymbol{\xi}))s)}}{\sqrt{1-s^2}(\beta+\sqrt{1-s^2})}\,\mathrm{d}s. \tag{7}$$

The variable s will be understood as $\sin\theta$ and $\sqrt{1-s^2}$ as $\cos\theta$. Since for reflected waves $\cos\theta \geqslant 0$ the positive $\sqrt{1-s^2}$ is taken such that $\mathrm{Re}\,(\sqrt{1-s^2}), \mathrm{Im}\,(\sqrt{1-s^2}) \geqslant 0$. Upon replacing s by $-s$ in equation (7), one concludes that the sign of the difference $(x(\mathbf{x}) - x(\boldsymbol{\xi}))$ is irrelevant and equation (7) can be written as

$$G_\beta(\boldsymbol{\xi}, \mathbf{x}) = \frac{\mathrm{i}\beta}{2\pi}\int_{-\infty}^{+\infty} \frac{\mathrm{e}^{\mathrm{i}k(\sqrt{1-s^2}(y(\mathbf{x})+y(\boldsymbol{\xi})) + |x(\mathbf{x})-x(\boldsymbol{\xi})|s)}}{\sqrt{1-s^2}(\beta+\sqrt{1-s^2})}\,\mathrm{d}s. \tag{8}$$

For application of the boundary element method, it is also necessary to evaluate the normal derivative of the correction term,

$$\frac{\partial G_\beta(\boldsymbol{\xi}, \mathbf{x})}{\partial \mathbf{n}(\mathbf{x})} = \frac{\partial G_\beta(\boldsymbol{\xi}, \mathbf{x})}{\partial x(\mathbf{x})}\,n_1 + \frac{\partial G_\beta(\boldsymbol{\xi}, \mathbf{x})}{\partial y(\mathbf{x})}\,n_2, \tag{9}$$

with n_1 and n_2 the components of the unit normal vector $\mathbf{n}$ at $\mathbf{x}$. Differentiating equation (7) with respect to $y(\mathbf{x})$, one has [11]

$$\partial G_\beta(\boldsymbol{\xi}, \mathbf{x})/\partial y(\mathbf{x}) = -(k\beta/2)\mathrm{H}_0^{(1)}(kr') - \mathrm{i}k\beta G_\beta(\boldsymbol{\xi}, \mathbf{x}), \tag{10}$$

which can easily be calculated once $G_\beta(\xi, \mathbf{x})$ is known. The term $\partial G_\beta(\xi, \mathbf{x})/\partial x(\mathbf{x})$ is also obtained by differentiating equation (7):

$$\frac{\partial G_\beta(\xi, \mathbf{x})}{\partial x(\mathbf{x})} = \frac{k\beta}{2\pi} \int_{-\infty}^{+\infty} \frac{s e^{ik(\sqrt{1-s^2}(y(\mathbf{x}) + y(\xi)) - (x(\mathbf{x}) - x(\xi))s)}}{\sqrt{1-s^2}(\beta + \sqrt{1-s^2})} \, ds. \tag{11}$$

Upon replacing s by $-s$ one concludes that equation (11) can be rewritten in the form

$$\frac{\partial G_\beta(\xi, \mathbf{x})}{\partial x(\mathbf{x})} = -\text{sign}\,(x(\mathbf{x}) - x(\xi)) \frac{k\beta}{2\pi} \int_{-\infty}^{+\infty} \frac{s e^{ik(\sqrt{1-s^2}(y(\mathbf{x}) + y(\xi)) + |x(\mathbf{x}) - x(\xi)|s)}}{\sqrt{1-s^2}(\beta + \sqrt{1-s^2})} \, ds. \tag{12}$$

The Green function correction term $G_\beta(\xi, \mathbf{x})$ and its normal derivative $\partial G_\beta(\xi, \mathbf{x})/\partial \mathbf{n}(\mathbf{x})$ for acoustic propagation in a half-space domain bounded by an impedance plane boundary (see Figure 1) are now established. For application of the dual boundary element method [16] over the non-thickness barrier, in which a hypersingular integral equation is also employed, an extra differentiation of the Green function and its normal derivative has to be performed with respect to the normal direction $\mathbf{m}$ at the collocation point ξ. The following functions appear in the hypersingular boundary integral equation, as will be shown in the next section:

$$\partial G(\xi, \mathbf{x})/\partial \mathbf{m}(\xi) = \partial G_o(\xi, \mathbf{x})/\partial \mathbf{m}(\xi) + \partial G_\beta(\xi, \mathbf{x})/\partial \mathbf{m}(\xi), \tag{13}$$

$$\partial^2 G(\xi, \mathbf{x})/\partial \mathbf{m}(\xi)\partial \mathbf{n}(\mathbf{x}) = \partial^2 G_o(\xi, \mathbf{x})/\partial \mathbf{m}(\xi)\partial \mathbf{n}(\mathbf{x}) + \partial^2 G_\beta(\xi, \mathbf{x})/\partial \mathbf{m}(\xi)\partial \mathbf{n}(\mathbf{x}). \tag{14}$$

Obtaining expressions for the first term on the right side of equations (13) and (14), and their numerical evaluation is straightforward. The last term in each of these equations can be expanded to

$$\frac{\partial G_\beta(\xi, \mathbf{x})}{\partial \mathbf{m}(\xi)} = \frac{\partial G_\beta(\xi, \mathbf{x})}{\partial x(\xi)} m_1 + \frac{\partial G_\beta(\xi, \mathbf{x})}{\partial y(\xi)} m_2 \tag{15}$$

and

$$\frac{\partial^2 G_\beta(\xi, \mathbf{x})}{\partial \mathbf{m}(\xi)\partial \mathbf{n}(\mathbf{x})} = \frac{\partial^2 G_\beta(\xi, \mathbf{x})}{\partial x(\xi)\partial x(\mathbf{x})} m_1 n_1 + \frac{\partial^2 G_\beta(\xi, \mathbf{x})}{\partial y(\xi)\partial x(\mathbf{x})} m_2 n_1 + \frac{\partial^2 G_\beta(\xi, \mathbf{x})}{\partial x(\xi)\partial y(\mathbf{x})} m_1 n_2 + \frac{\partial^2 G_\beta(\xi, \mathbf{x})}{\partial y(\xi)\partial y(\mathbf{x})} m_2 n_2, \tag{16}$$

with m_1 and m_2 the direction cosines of the unit normal $\mathbf{m}(\xi)$. It is easy to see, from the integral in equation (7), that

$$\partial G_\beta(\xi, \mathbf{x})/\partial x(\xi) = -\partial G_\beta(\xi, \mathbf{x})/\partial x(\mathbf{x}) \qquad \text{and} \qquad \partial G_\beta(\xi, \mathbf{x})/\partial y(\xi) = -\partial G_\beta(\xi, \mathbf{x})/\partial y(\mathbf{x}). \tag{17, 18}$$

Therefore, $\partial G_\beta(\xi, \mathbf{x})/\partial \mathbf{m}(\xi)$ can be evaluated from expressions obtained for the standard boundary integral equation. The terms on the right side of equation (16) are analyzed separately. The last one is given by differentiating equation (10) with respect to $y(\xi)$, and the result is

$$\frac{\partial^2 G_\beta(\xi, \mathbf{x})}{\partial y(\xi)\partial y(\mathbf{x})} = \frac{ik^2\beta^2}{2} H_0^{(1)}(kr') + \frac{k^2\beta}{2} \frac{(y(\mathbf{x}) + y(\xi))}{r'} H_1^{(1)}(kr') - k^2\beta^2 G_\beta(\xi, \mathbf{x}). \tag{19}$$

The third term is obtained by differentiating equation (10) with respect to $x(\xi)$:

$$\frac{\partial^2 G_\beta(\xi, \mathbf{x})}{\partial x(\xi)\partial y(\mathbf{x})} = -\frac{k^2\beta}{2} \frac{(x(\mathbf{x}) - x(\xi))}{r'} H_1^{(1)}(kr') + ik\beta \frac{\partial G_\beta(\xi, \mathbf{x})}{\partial x(\mathbf{x})}. \tag{20}$$

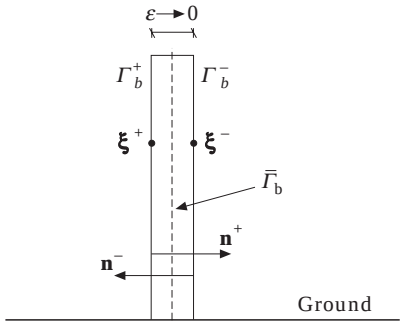

Figure 2. The thin barrier geometry.

The second can be shown to be equal to the negative of the third,

$$\partial^2 G_\beta(\boldsymbol{\xi}, \mathbf{x})/\partial y(\boldsymbol{\xi})\partial x(\mathbf{x}) = -\partial^2 G_\beta(\boldsymbol{\xi}, \mathbf{x})/\partial x(\boldsymbol{\xi})\partial y(\mathbf{x}), \tag{21}$$

while the first term is obtained by differentiating equation (7) with respect to $x(\boldsymbol{\xi})$, and using some algebraic manipulation:

$$\frac{\partial^2 G_\beta(\boldsymbol{\xi}, \mathbf{x})}{\partial x(\boldsymbol{\xi})\partial x(\mathbf{x})} = \frac{\mathrm{i}k^2\beta^2}{2}\,\mathrm{H}_0^{(1)}(kr') + \frac{k^2\beta}{2}\,\frac{(y(\mathbf{x}) + y(\boldsymbol{\xi}))}{r'}\,\mathrm{H}_1^{(1)}(kr') + k^2(1-\beta^2)G_\beta(\boldsymbol{\xi}, \mathbf{x}). \tag{22}$$

Consequently, the function $\partial^2 G_\beta(\boldsymbol{\xi}, \mathbf{x})/\partial \mathbf{m}(\boldsymbol{\xi})\partial \mathbf{n}(\mathbf{x})$ can also be computed once the correction term $G_\beta(\boldsymbol{\xi}, \mathbf{x})$ and its derivative with respect to $x(\mathbf{x})$ are known.

3. DUAL BEM FORMULATION FOR NON-THICKNESS BARRIER

By applying Green's second identity to the boundary value problem stated by equations (1)–(3), the following integral equation is obtained for collocation points inside the domain Ω:

$$\phi(\boldsymbol{\xi}) = \int_{\Gamma_g + \Gamma_b} \left\{ G(\boldsymbol{\xi}, \mathbf{x})q(\mathbf{x}) - \frac{\partial G(\boldsymbol{\xi}, \mathbf{x})}{\partial \mathbf{n}(\mathbf{x})}\,\phi(\mathbf{x}) \right\} \mathrm{d}\Gamma + \phi_I(\boldsymbol{\xi}). \tag{23}$$

Here $\phi_I(\boldsymbol{\xi})$ is the known incident wave contribution coming from monofrequency concentrated sources. By taking the collocation point $\boldsymbol{\xi}$ to the boundary Γ via a limiting process, and recalling that the Green function $G(\boldsymbol{\xi}, \mathbf{x})$ satisfies the boundary condition (2) over Γ_g, a standard boundary integral equation (SBIE) is found in the form

$$\tfrac{1}{2}\phi(\boldsymbol{\xi}) = \int_{\Gamma_b} G(\boldsymbol{\xi}, \mathbf{x})q(\mathbf{x})\,\mathrm{d}\Gamma - \int_{\Gamma_b} \frac{\partial G(\boldsymbol{\xi}, \mathbf{x})}{\partial \mathbf{n}(\mathbf{x})}\,\phi(\mathbf{x})\,\mathrm{d}\Gamma + \phi_I(\boldsymbol{\xi}). \tag{24}$$

The integral equation (24) has been employed by Chandler-Wilde and Hothersall [6], and more recently by Park and Eversman [10], for the study of acoustic barriers over impedance planes. In order to use the BEM, the contour Γ_b is discretized into N_b elements over which the discretized form of equation (24) is applied to generate a system of N_b equations and N_b unknowns (it being assumed that simple constant elements are used).

Now consider a barrier with its thickness tending to zero, as shown in Figure 2. The application of the integral equation (24) over the boundaries Γ_b^+ and Γ_b^-, which comprise

the barrier vertical face and one-half of the top horizontal face, generates the equations

$$\tfrac{1}{2}\phi^+(\xi^+) = \int_{\Gamma_b^+} G(\xi^+, \mathbf{x}) q^+(\mathbf{x})\, \mathrm{d}\Gamma + \int_{\Gamma_b^-} G(\xi^+, \mathbf{x}) q^-(\mathbf{x})\, \mathrm{d}\Gamma$$

$$- \int_{\Gamma_b^+} \frac{\partial G(\xi^+, \mathbf{x})}{\partial \mathbf{n}^+(\mathbf{x})}\, \phi^+(\mathbf{x})\, \mathrm{d}\Gamma - \int_{\Gamma_b^-} \frac{\partial G(\xi^+, \mathbf{x})}{\partial \mathbf{n}^-(\mathbf{x})}\, \phi^-(\mathbf{x})\, \mathrm{d}\Gamma + \phi_I(\xi^+) \tag{25}$$

and

$$\tfrac{1}{2}\phi^-(\xi^-) = \int_{\Gamma_b^+} G(\xi^-, \mathbf{x}) q^+(\mathbf{x})\, \mathrm{d}\Gamma + \int_{\Gamma_b^-} G(\xi^-, \mathbf{x}) q^-(\mathbf{x})\, \mathrm{d}\Gamma$$

$$- \int_{\Gamma_b^+} \frac{\partial G(\xi^-, \mathbf{x})}{\partial \mathbf{n}^+(\mathbf{x})}\, \phi^+(\mathbf{x})\, \mathrm{d}\Gamma - \int_{\Gamma_b^-} \frac{\partial G(\xi^-, \mathbf{x})}{\partial \mathbf{n}^-(\mathbf{x})}\, \phi^-(\mathbf{x})\, \mathrm{d}\Gamma + \phi_I(\xi^-). \tag{26}$$

Equations (25) and (26) together are equivalent to equation (24). They can be applied to solve problems with thin barriers but fine discretizations (comparable to the thickness of the structure) must always be used, even for low frequencies, to avoid the near-degenerate system of equations as well as the near-singular integrations. The first problem arises when the thickness is very small as the equation produced for ξ^+ is nearly the same as the one for ξ^- at the same height in the barrier. The second is evident when the element to be integrated is at one side and the collocation point is just opposite to it at the other. Depending on the problem to be analyzed this refinement may be very costly in terms of computer time and memory, especially in 3-D cases.

In the limit when $\varepsilon \to 0$, Γ_b^+ and Γ_b^- occupy the same position $\bar{\Gamma}_b$, $\mathbf{n}^+(\mathbf{x}) = -\mathbf{n}(\mathbf{x})$, $\mathbf{n}^-(\mathbf{x}) = \mathbf{n}(\mathbf{x})$ and the boundary integral equation for a collocation point on any side of the barrier will be [14]

$$\tfrac{1}{2}\Sigma\phi(\xi) + \int_{\bar{\Gamma}_b} G(\xi, \mathbf{x}) \Delta\hat{q}(\mathbf{x})\, \mathrm{d}\Gamma = \int_{\bar{\Gamma}_b} \frac{\partial G(\xi, \mathbf{x})}{\partial \mathbf{n}(\mathbf{x})}\, \Delta\phi(\mathbf{x})\, \mathrm{d}\Gamma + \phi_I(\xi), \tag{27}$$

where $\Sigma\phi(\xi) = \phi^+(\xi) + \phi^-(\xi)$, $\Delta\phi(\mathbf{x}) = \phi^+(\mathbf{x}) - \phi^-(\mathbf{x})$, $\Delta\hat{q}(\mathbf{x}) = \hat{q}^+(\mathbf{x}) - \hat{q}^-(\mathbf{x})$, $\hat{q}^+(\mathbf{x}) = \partial\phi^+(\mathbf{x})/\partial\mathbf{n}(\mathbf{x})$ and $\hat{q}^-(\mathbf{x}) = \partial\phi^-(\mathbf{x})/\partial\mathbf{n}(\mathbf{x})$. Applying equation (27) over N_b elements produces twice more unknowns than equations. In order to overcome this difference a hypersingular boundary integral equation (HBIE), to be derived next, is also applied along the barrier.

Before applying the HBIE to the non-thickness boundary it is interesting to confirm that this new integral equation, like the SBIE, behaves in such a way that the integration over the plane impedance ground Γ_g does not need to be evaluated. The HBIE can be obtained by differentiating equation (23) with respect to $\mathbf{m}(\xi)$ and taking ξ to the boundary via a limiting process, giving

$$\tfrac{1}{2}q(\xi) = \int_{\Gamma_g + \Gamma_b} \left\{ \mathrm{i}k\beta \frac{\partial G(\xi, \mathbf{x})}{\partial \mathbf{m}(\xi)} - \frac{\partial^2 G(\xi, \mathbf{x})}{\partial \mathbf{m}(\xi) \partial \mathbf{n}(\mathbf{x})} \right\} \phi(\mathbf{x})\, \mathrm{d}\Gamma + \frac{\partial \phi_I(\xi)}{\partial \mathbf{m}(\xi)}. \tag{28}$$

Calling the term in brackets I and substituting in it equations (13) and (14), one has

$$I = \mathrm{i}k\beta\left(\frac{\partial G_o(\boldsymbol{\xi}, \mathbf{x})}{\partial \mathbf{m}(\boldsymbol{\xi})} + \frac{\partial G_\beta(\boldsymbol{\xi}, \mathbf{x})}{\partial \mathbf{m}(\boldsymbol{\xi})}\right) - \frac{\partial^2 G_o(\boldsymbol{\xi}, \mathbf{x})}{\partial \mathbf{m}(\boldsymbol{\xi})\partial \mathbf{n}(\mathbf{x})} - \frac{\partial^2 G_\beta(\boldsymbol{\xi}, \mathbf{x})}{\partial \mathbf{m}(\boldsymbol{\xi})\partial \mathbf{n}(\mathbf{x})}. \tag{29}$$

The third term disappears because $\partial G_o(\boldsymbol{\xi}, \mathbf{x})/\partial \mathbf{n}(\mathbf{x})$ is zero at Γ_g due to the application of the method of images in the SBIE. Also, at Γ_g, $\mathbf{n}(\mathbf{x}) = -y(\mathbf{x})$ and the fourth term can be represented by

$$\frac{\partial^2 G_\beta(\boldsymbol{\xi}, \mathbf{x})}{\partial \mathbf{m}(\boldsymbol{\xi})\partial y(\mathbf{x})} = \frac{\partial}{\partial \mathbf{m}(\boldsymbol{\xi})}\left(\frac{-k\beta}{2}\,\mathrm{H}_0^{(1)}(kr')\right) - \mathrm{i}k\beta\,\frac{\partial G_\beta(\boldsymbol{\xi}, \mathbf{x})}{\partial \mathbf{m}(\boldsymbol{\xi})}. \tag{30}$$

Substituting expression (30) into equation (29), as well as the derivative $\partial G_o(\boldsymbol{\xi}, \mathbf{x})/\partial \mathbf{m}(\boldsymbol{\xi})$, one finds that $I = 0$. This result confirms that the expressions for derivatives of $G_\beta(\boldsymbol{\xi}, \mathbf{x})$ are correct and also that the discretization of Γ_g is not necessary. Thus, the HBIE is written in the form

$$\tfrac{1}{2}q(\boldsymbol{\xi}) = \int_{\Gamma_b} \frac{\partial G(\boldsymbol{\xi}, \mathbf{x})}{\partial \mathbf{m}(\boldsymbol{\xi})}\, q(\mathbf{x})\, \mathrm{d}\Gamma - \text{⨍}\!\!\!\!\!\!\int_{\Gamma_b} \frac{\partial^2 G(\boldsymbol{\xi}, \mathbf{x})}{\partial \mathbf{m}(\boldsymbol{\xi})\partial \mathbf{n}(\mathbf{x})}\, \phi(\mathbf{x})\, \mathrm{d}\Gamma + \frac{\partial \phi_I(\boldsymbol{\xi})}{\partial \mathbf{m}(\boldsymbol{\xi})}. \tag{31}$$

The sign in the second integral indicates its interpretation as a Hadamard finite part integral [17]. As was shown for the SBIE, the near-degeneracy problem in the analysis of thin barriers, as well as degeneracy in non-thickness ones, are also present if the HBIE is used alone.

The HBIE for non-thickness problems is obtained by differentiating equation (23) with respect to $\mathbf{m}(\boldsymbol{\xi})$, applying the limit when $\varepsilon \to 0$ and finally taking $\boldsymbol{\xi}$ to the boundary via a limiting process, giving

$$\tfrac{1}{2}\Sigma\hat{q}(\boldsymbol{\xi}) + \int_{\Gamma_b} \frac{\partial G(\boldsymbol{\xi}, \mathbf{x})}{\partial \mathbf{m}(\boldsymbol{\xi})}\, \Delta\hat{q}(\mathbf{x})\, \mathrm{d}\Gamma = \text{⨍}\!\!\!\!\!\!\int_{\Gamma_b} \frac{\partial^2 G(\boldsymbol{\xi}, \mathbf{x})}{\partial \mathbf{m}(\boldsymbol{\xi})\partial \mathbf{n}(\mathbf{x})}\, \Delta\phi(\mathbf{x})\, \mathrm{d}\Gamma + \frac{\partial \phi_I(\boldsymbol{\xi})}{\partial \mathbf{m}(\boldsymbol{\xi})}, \tag{32}$$

where $\Sigma\hat{q}(\boldsymbol{\xi}) = \hat{q}^+(\mathbf{x}) + \hat{q}^-(\mathbf{x})$. The dual boundary element method basically consists of the application of equations (27) and (32), one on each side of the non-thickness barrier, in order to generate a well-conditioned system of equations.

In problems in which the barrier is rigid at both sides, the dual BE method has an extra advantage in that the system of equations to be solved is half the size of the one obtained from the conventional method. Since $\Sigma\hat{q}$ and $\Delta\hat{q}$ are zero in this case, the hypersingular equation (32) can initially be solved to obtain $\Delta\phi(\mathbf{x})$ and, afterwards, the values of $\phi(\mathbf{x})$ at each side of the barrier are directly computed with the standard equation (27).

When the barrier surfaces are covered with absorbing material, the boundary conditions

$$\hat{q}^+(\mathbf{x}) = -\mathrm{i}k\beta^+(\mathbf{x})\phi^+(\mathbf{x}), \qquad \text{and} \qquad \hat{q}^-(\mathbf{x}) = \mathrm{i}k\beta^-(\mathbf{x})\phi^-(\mathbf{x}) \tag{33, 34}$$

are applied to equations (27) and (32) and the system obtained by collocating these equations at all boundary nodes can be solved to produce the values of potential at both sides of the barrier (i.e., ϕ^+ and ϕ^-). The variables $\beta^+(\mathbf{x})$ and $\beta^-(\mathbf{x})$ are the surface admittances at the front and back of the barrier, respectively. In this paper, they are calculated according to the Delany–Bazley model [18], where each surface consists of a hard-backed layer of finite thickness. The correction terms depend on the value of the ground normalized admittance β, which is also calculated with this model considering the ground as an infinitely thick porous layer.

The computation of potential values at field points is carried out with equation (27) where the first term $\frac{1}{2}\Sigma\phi(\boldsymbol{\xi})$ is replaced by $\phi(\boldsymbol{\xi})$ and the integration is carried over $\overline{\Gamma}_b$.

4. NUMERICAL ASPECTS

The evaluation of integrals of the Green function and its derivatives is performed numerically by using Gaussian quadrature. The number of points employed for integration over each element depends on the size of the element compared to its distance from the collocation point. This number should always be kept to a minimum necessary due to the expensive computation of the correction term and its x-derivative when $\beta \neq 0$.

In two-dimensional problems such as this, computation of the integrals is usually more time consuming than the solution of the system. It can be seen, before applying boundary conditions, that the standard formulation (equation (24)) produces fully populated matrices for the variables ϕ^+, ϕ^-, q^+ and q^-, where each matrix coefficient corresponds to an element integral. On the other hand, the dual formulation (equations (27, 32)) produces matrices for the variables $\Sigma\phi$, $\Delta\phi$, $\Delta\hat{q}$ and $\Sigma\hat{q}$ which are approximately of the same size as those in the standard formulation but with only half of each populated with element integrals. Also, in a thick barrier each integration point belongs to one single element and $G_\beta(\boldsymbol{\xi}, \mathbf{x})$ and its x-derivative have to be calculated at each of them, while in a non-thickness barrier, each integration point geometrically belongs to two elements (one of each side), so the evaluation of the contribution of each point is performed at the same time for both standard and hypersingular equations. For those reasons, a reduction of approximately 75% is expected in the required computing time for this task. Also, nearly 50% reduction in time should be obtained in the computation of field points.

A non-dimensional limit of 23 was chosen for kr', such that for values of kr' above this limit asymptotic expressions are used; otherwise, numerical quadrature is used [6]. This choice guarantees errors from the asymptotic expressions smaller than 10^{-5}. Asymptotic expressions are obtained following the work of Kawai *et al*. [5].

Numerical quadrature is used for $kr' < 23$ with a variable number of Gaussian points, after the path of integration is deformed to the steepest descent path. Depending on the values of β and θ_o (see Figure 1), a pole may lie near the path of integration. The closer to the path, the steeper is the behaviour of the integrands and the more difficult is their evaluation. In steepest cases 60 Gaussian points are used over the path which is divided into three segments. Over each segment, 20 points are used and rearranged with a third degree co-ordinate transformation [19]. In other cases, that are not so steep, the same subdivision is applied but a smaller number of Gauss points is sufficient to maintain the same margin of error established with the non-dimensional value $kr' = 23$.

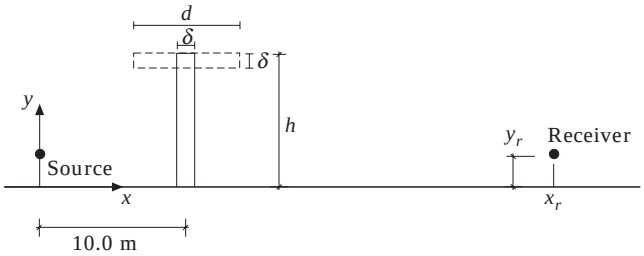

Figure 3. The geometry of the tests.

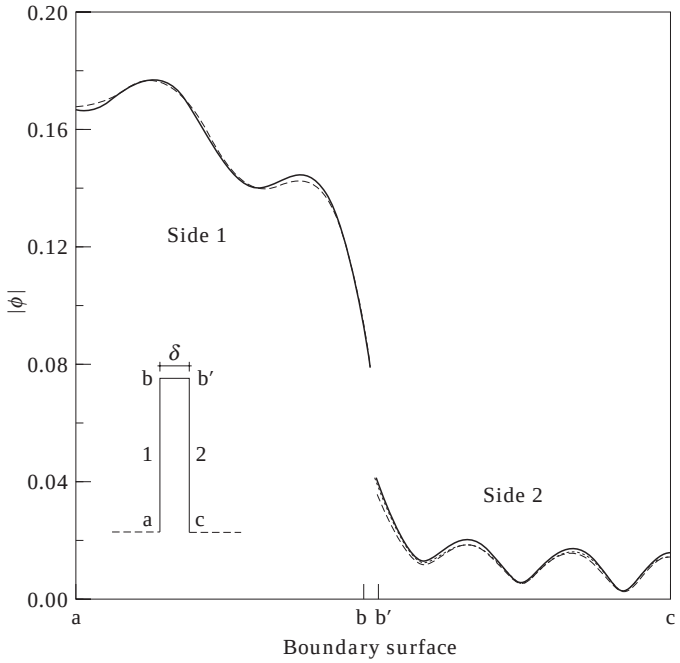

Figure 4. The velocity potential modulus at a rigid vertical barrier for a frequency of 100 Hz. δ-values: ——, dual; ---, 5 cm; – – –, 20 cm.

5. NUMERICAL TESTS

All of the tests shown in this section involve a comparison of results from the proposed dual formulation ($\delta = 0{\cdot}0$ m) with the conventional method for two different barrier thicknesses ($\delta = 0{\cdot}05$ m and $\delta = 0{\cdot}20$ m). A minimum of eight constant elements per wavelength was used in all analyses.

Consider a plane vertical barrier with height $h = 5{\cdot}0$ m located over a plane boundary, as shown in Figure 3. A unit monofrequency source is located 10·0 m from the barrier and 1·0 m above the ground, which has a normalized admittance characterized by a flow resistivity $\sigma = 300\,000$ N sm^{-4} (grassland) and the frequency of the source.

In the first test, values of the velocity potential modulus at a vertical barrier are computed when the source has a frequency of 100 Hz and the barrier is considered rigid on both sides. Excellent agreement is shown in Figure 4 between the SBIE and the proposed dual formulation in this example. A similar analysis was carried out for a rigid T-shaped barrier (indicated in Figure 3) with a cap width $d = 2{\cdot}0$ m. The results shown in Figure 5 are generally very good, although some small differences are evident, especially in side 1 of the barrier. From this result it is clear that the dual solution is closer to the 5 cm solution than this one is to the 20 cm solution, indicating convergence. As explained at the end of section 3, the previous rigid barrier problems were analyzed more efficiently with the dual method in terms of computer time and memory. This efficiency is proportional to the frequency, and it is for higher source frequencies that the computational advantage is more significant.

The third example has the same general configuration of the first, except that now the barrier has different surface treatments on its front and back sides. The front side is covered with a material characterized by $\sigma = 20\,000$ N sm^{-4} with a depth of 0·1 m, while the back side is considered to be rigid. The acoustic potential values at the barrier are shown in

Figure 6, confirming the good agreement for different boundary conditions. Also, from this analysis, values of insertion loss (*IL*) at field points were computed. The field points were positioned at $y_r = 1{\cdot}5$ m and x_r varying from 0·0 m to 60·0 m. The computed results are shown in Figure 7, in which a few discrepancies can be observed before the barrier, between the 20 cm solution and the other two. After the barrier, which is the main region of interest, all solutions agree very well, especially the dual and the 5 cm ones.

In the last test, the same vertical barrier with a front surface treatment, but now with height $h = 4{\cdot}0$ m is analyzed for a range of frequencies between 63 Hz and 4000 Hz. The values of insertion loss at a field point located at $x_r = 40{\cdot}0$ m, $y_r = 1{\cdot}80$ m are plotted in Figure 8. Very good agreement was achieved, even for higher frequencies where the wavelength is comparable to the thickness of the barrier. Small differences between solutions can again be observed mainly for frequencies above 1750 Hz. Once more, the dual and the 5 cm conventional solution are close to one another even in this range of higher frequencies.

In Table 1 a comparison is shown between computing times required by the standard and dual formulations in five different frequencies. As expected, an average reduction of 75% was achieved in the system assembling. It can also be seen that the total reduction (assembling + solving) was still very high, since the assembling for this problem is very time consuming. The system of equations was solved by Gauss elimination. Although this direct solver is efficient for small systems of equations, its cost becomes comparable to that of assembling for higher frequencies where iterative solvers should be preferred.

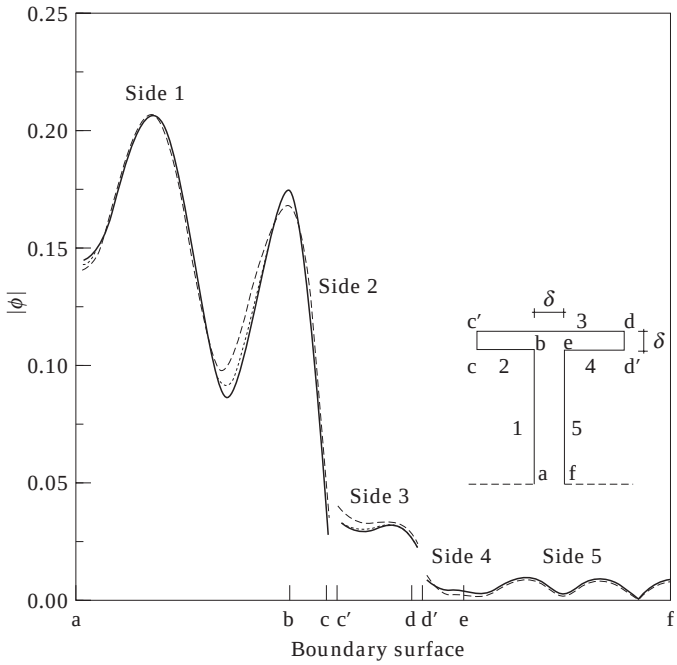

Figure 5. The velocity potential modulus at a rigid T-shaped barrier for a frequency of 100 Hz. Key as Figure 4.

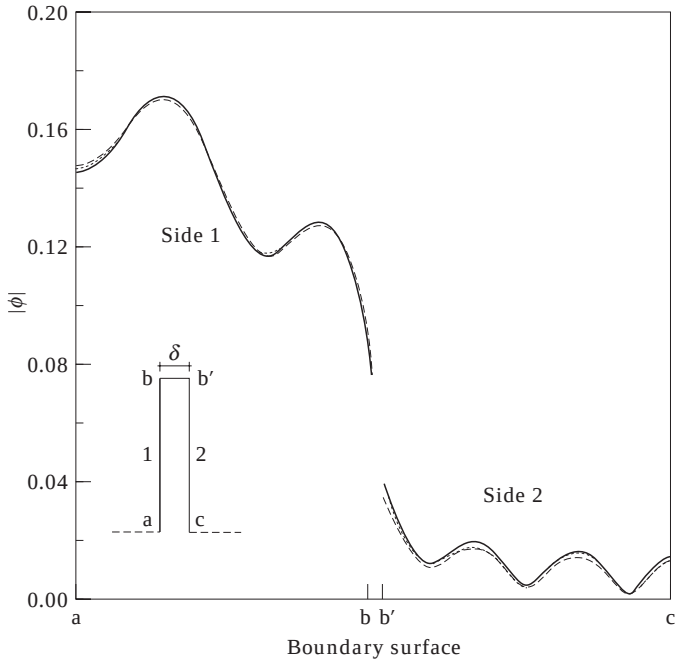

Figure 6. The velocity potential modulus at a vertical barrier with different surface treatments on each side, for a frequency of 100 Hz. Key as Figure 4.

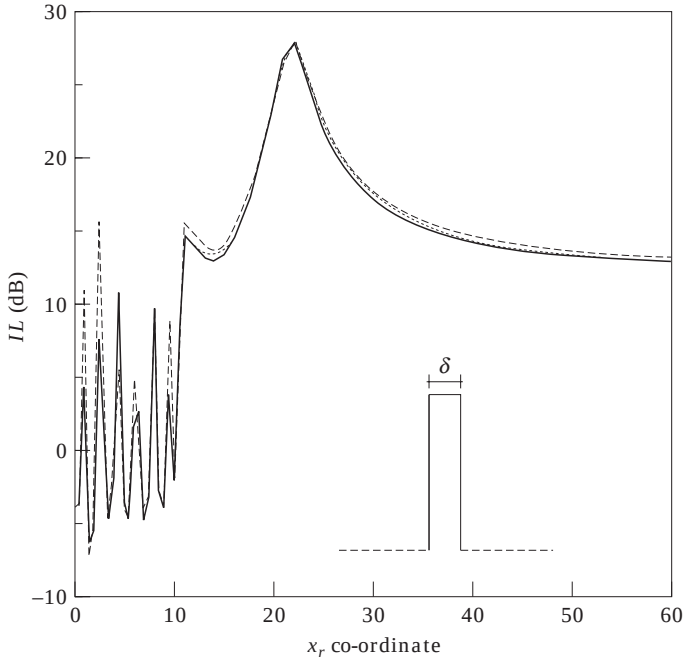

Figure 7. The insertion loss at field points 1·5 m above the ground between 0·0 m and 60·0 m, for a frequency of 100 Hz. Key as Figure 4.

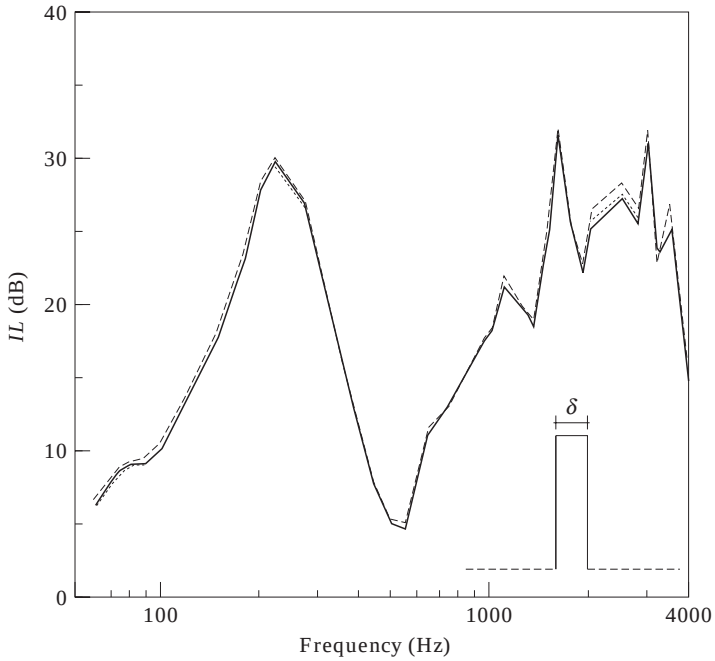

Figure 8. The insertion loss at a field point located at (40·0, 1·8) for frequencies between 63 and 4000 Hz. Key as Figure 4.

TABLE 1

Time comparisons between standard (0·2 *m*) *and dual formulations*

Frequency (Hz)	System assembling (s)			System solving (s)			Total reduction (%)
	SBEM	Dual	Reduction (%)	SBEM	Dual	Reduction (%)	
100	10·9	2·6	76·1	—	—	—	76·1
500	88·2	23·6	73·2	1·8	1·6	11·1	72·0
1000	255·1	65·4	74·4	13·3	12·4	6·8	71·0
2000	911·2	226·9	75·1	103·1	95·9	7·0	68·2
4000	3444·5	883·4	74·4	817·9	759·1	7·2	61·5

6. CONCLUSIONS

In this paper a dual boundary element formulation has been presented for studying sound propagation around acoustic barriers over a homogeneous impedance plane. The dual BE formulation involves the application of two integral equations (the standard Helmholtz integral representation and its hypersingular counterpart) over a non-thickness barrier. The Green function employed directly incorporates the plane absorbing ground, so the only necessary discretization is that over the barrier axis.

Several tests were performed to assess the theoretical and numerical developments. In all tests, comparisons with results obtained with barriers of thickness 5 cm and 20 cm confirmed that the numerical results always converged to the non-thickness case, attesting the correctness of the theoretical formulation and its related numerical algorithms. It was also shown that, in almost all of the cases studied, the difference in results between a 5 cm barrier and a non-thickness one was invariably very small.

It is concluded that the dual BE formulation is very effective and accurate for the analysis of thin barriers. The present research is now being extended to three-dimensional problems, in which case substantial savings in computer time and memory should be expected.

ACKNOWLEDGMENTS

We thank Dr H. Power of the Wessex Institute of Technology for many helpful discussions. The first author would like to acknowledge the financial support provided by CAPES, Ministry of Education, Brazil.

REFERENCES

1. R. Seznec 1980 *Journal of Sound and Vibration* **73**, 195–209. Diffraction of sound around barriers: use of the boundary elements technique.
2. A. R. Wenzel 1974 *Journal of the Acoustical Society of America* **55**, 956–963. Propagation of waves along an impedance boundary.
3. C. F. Chien and W. W. Soroka 1975 *Journal of Sound and Vibration* **43**, 9–20. Sound propagation along an impedance plane.
4. S. I. Thomasson 1976 *Journal of the Acoustical Society of America* **59**, 780–785. Reflection of waves from a point source by an impedance boundary.
5. T. Kawai, T. Hidaka and T. Nakajima 1982 *Journal of Sound and Vibration* **83**, 125–138. Sound propagation above an impedance boundary.
6. S. N. Chandler-Wilde and D. C. Hothersall 1985 *Journal of Sound and Vibration* **98**, 475–491. Sound propagation above an inhomogeneous impedance plane.
7. P. C. Clemmow 1950 *Quarterly Journal of Mechanics and Applied Mathematics* **3**, 241–256. Some extensions to the method of integration by steepest descents.
8. L. M. Brekhovskikh 1960 *Waves in Layered Media*. New York: Academic Press.
9. D. C. Hothersall, S. N. Chander-Wilde and N. M. Hajmirzae 1991 *Journal of Sound and Vibration* **146**, 303–322. The efficiency of single noise barriers.
10. J. M. Park and W. Eversman 1994 *Journal of Sound and Vibration* **175**, 197–218. A boundary element method for propagation over absorbing boundaries.
11. S. N. Chandler-Wilde and D. C. Hothersall 1995 *Journal of Sound and Vibration* **180**, 705–724. Efficient calculation of the Green function for acoustic propagation above a homogeneous impedance plane.
12. T. Terai 1980 *Journal of Sound and Vibration* **69**, 71–100. On calculation of sound field around three dimensional objects by integral equation methods.
13. L. J. Gray 1989 *Engineering Analysis with Boundary Elements* **6**, 180–184. Boundary element methods for regions with thin internal cavities.
14. G. Krishnasamy, F. J. Rizzo and Y. Liu 1994 *International Journal for Numerical Methods in Engineering* **37**, 107–121. Boundary integral equations for thin bodies.
15. P. J. T. Filippi 1977 *Journal of Sound and Vibration* **54**, 473–500. Layer potentials and acoustic diffraction.
16. A. Portela, M. H. Aliabadi and D. P. Rooke 1992 *International Journal for Numerical Methods in Engineering* **33**, 1269–1287. The dual boundary element method: effective implementation for crack problems.
17. J. Hadamard 1923 *Lectures on Cauchy's Problem in Linear Partial Differential Equations*. New Haven, CT: Yale University Press.
18. M. E. Delany and E. N. Bazley 1970 *Applied Acoustics* **3**, 105–116. Acoustical properties of fibrous absorbent materials.
19. J. C. F. Telles 1987 *International Journal for Numerical Methods in Engineering* **24**, 959–973. A self-adaptive co-ordinate transformation for efficient numerical evaluation of general boundary element integrals.
20. D. C. Hothersall, D. H. Crombie and S. N. Chandler-Wilde 1991 *Applied Acoustics* **32**, 269–287. The performance of T-profile and associated noise barriers.